

Phase Compensation Techniques for Low-Power Operational Amplifiers

Rui ITO^{†a)} and Tetsuro ITAKURA^{††b)}, Members

SUMMARY An operational amplifier is one of the key functional blocks and is widely used in analog and mixed-signal circuits. For low-power consumption, many techniques such as class AB and slew-rate enhancement have been proposed. Although phase compensation is related to power consumption, it has not been clearly discussed from the viewpoint of the power consumption. In this paper, the conventional and the improved Miller compensations and the phase compensation by introducing a new zero are discussed for low-power operational amplifiers.

key words: low-power, operational amplifier (opamp), phase-compensation

1. Introduction

The operational amplifier (opamp) is the most basic circuit in the analog circuit, and it has been widely used in many applications. For example, in cellular phones as shown in Fig. 1, the opamp is used in an audio, a microphone, a liquid crystal display (LCD) and a transceiver IC. In the direct conversion transceiver shown in Fig. 2, the opamp is used in the analog baseband circuits such as low-pass filter (LPF), variable gain amplifier (VGA) and analog/digital converter (ADC) [1]–[4]. In the LCD driver circuit shown in Fig. 3, the opamps are used for the buffer amplifiers that drive the signal lines on the LCD panel [5], [6]. Several hundred opamps are integrated in a single chip, the power consumption of opamps becomes dominant. In battery driven equipment such as a cellular phone, low-power consumption is required for expanding talk time and standby time. Much research has been done to reduce power consumption of opamps.

Class B [7], [8], class AB [9]–[14], push-pull [15], [16], dynamic bias (DB) [17], [18], dynamic amp (DA) [19], and slew-rate enhancement (SRE) [5], [20]–[22] have been reported for reducing the power consumption of opamps.

In the class B output stage, when there is no input signal, the current of the output stage becomes zero. Only when the input signal amplitude becomes larger than the predetermined value, the current of output stage increases according to the input signal amplitude. Since the power consumption depends on the input signal amplitude, the power con-

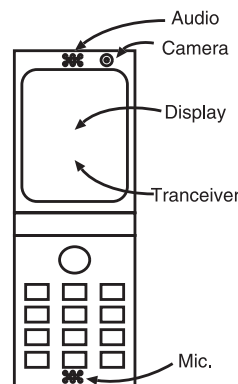


Fig. 1 Cellular phone.

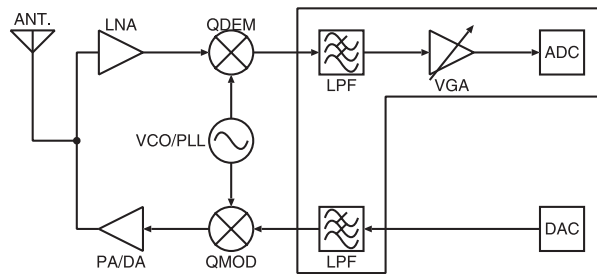


Fig. 2 Transceiver.

sumption of the opamp can be reduced. However, crossover distortion, which occurs for small input signal amplitudes, should be taken into account to achieve good linearity. Class AB output stage flows small bias current even when there is no or small input signal. This improves the linearity of the opamp. Class B and class AB are used in order to reduce the power consumption in LPF, VGA and the buffer that operate at continuous time.

DB and DA are used in the switched-capacitor (SC) circuits and sample-and-hold (SH) circuits that operate at discrete time. In these techniques, the bias current is applied to the opamp at clock rising or falling edges.

SRE is the technique for reducing the power consumption, which is also suitable for discrete-time applications such as SC circuits and LCD driver circuits. SRE senses the difference between the plus and the minus input voltages, and increases the bias current of the opamp when the difference is larger than the predetermined level.

The research on reducing the power consumption by improving the drive capability of the opamp has been dis-

Manuscript received March 4, 2010.

[†]The author is with System LSI Division Analog Device Design Dept., Toshiba Corporation Semiconductor Company, Kawasaki-shi, 212-8520 Japan.

^{††}The author is with Corporate Research & Development Center, Toshiba Corporation, Kawasaki-shi, 212-8582 Japan.

a) E-mail: rui.ito@toshiba.co.jp

b) E-mail: tetsuro.itakura@toshiba.co.jp

DOI: 10.1587/transele.E93.C.730

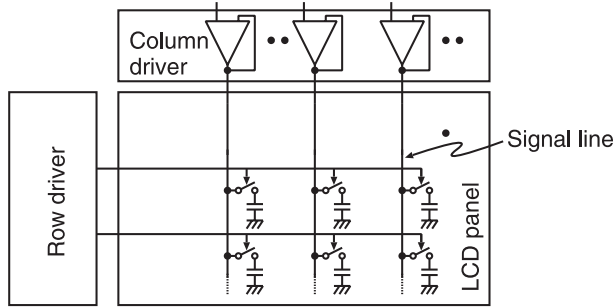


Fig. 3 LCD driver circuit.

cussed in many papers. On the other hand, the phase compensation has not been clearly discussed from the viewpoint of the reduction of the power consumption, although the improvement of the compensation and the reduction of the compensation capacitance have been reported in many papers [23]–[25]. For example, in the LCD driver circuits, the settling time is important and is affected by the slew rate, which the compensation capacitance and the bias current affect. So, the phase compensation is a crucial issue in the context of efforts to reduce the power consumption of the opamp. In the wideband wireless applications such as LTE [26] and WiMAX [27], the phase compensation of the opamp is also crucial to satisfy both wide bandwidth and low-power consumption.

In this paper, the phase compensation techniques are discussed from the viewpoint of reducing the power consumption.

2. Conventional and Improved Miller Compensation Techniques

The well-known phase compensation technique is the Miller compensation shown in Fig. 4. The small signal equivalent circuit of the Miller compensation is shown in Fig. 5. The transfer function, $H_{mil}(s)$, of the Miller compensation is obtained as follows;

$$H_{mil}(s) \approx A_{mil} \frac{1 - s/z_{mil}}{(1 - s/p_{1mil})(1 - s/p_{2mil})} \quad (1)$$

$$A_{mil} = \frac{g_{m1} g_{m2}}{g_{o1} g_{o2}} \quad (2)$$

$$p_{1mil} = -\frac{g_{o2} g_{o1}}{g_{m2} C_C} \quad (3)$$

$$p_{2mil} = -\frac{g_{m2} C_C}{C_L C_1 + C_L C_C + C_C C_1} \quad (4)$$

$$z_{mil} = \frac{g_{m2}}{C_C} \quad (5)$$

where A_{mil} is the total DC gain, p_{1mil} and p_{2mil} are the first and the second poles, z_{mil} is the zero, g_{m1} and g_{m2} are transconductances of the input and the output stages, g_{o1} and g_{o2} are the output conductance of the input and output stages, C_1 is the parasitic capacitance at the output of the input stage, C_C is the phase compensation capacitor, C_L is the load capacitance at the output, and I_1 and I_2 are the bias currents of

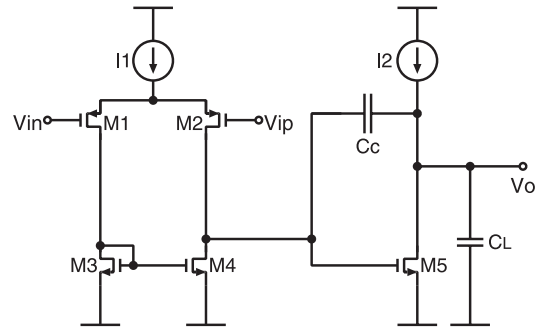


Fig. 4 Conventional Miller compensation.

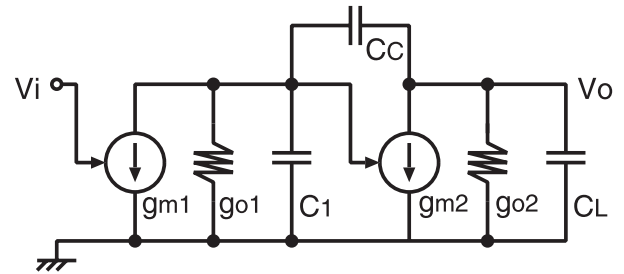


Fig. 5 Conventional Miller compensation (equivalent circuit).

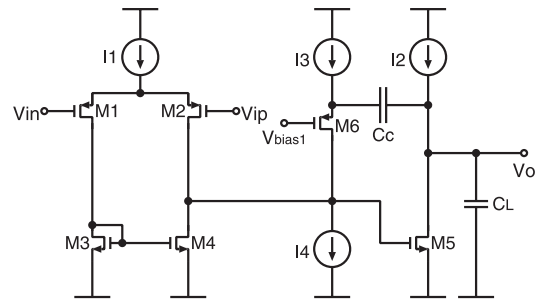


Fig. 6 Improved Miller compensation.

the input and the output stages. Assuming that the current drive-capability of the output stage is sufficiently high, the slew rate, SR_{mil} , of the opamp is limited as follows;

$$SR_{mil} = \frac{I_1}{C_C} \quad (6)$$

In order to achieve the stability of the opamp, it is necessary to guarantee the phase margin. For larger C_L , larger C_C and/or larger g_{m2} are required to achieve the same phase margin. Larger I_1 is also necessary for keeping the same slew rate for larger C_C .

The improved Miller compensation shown in Fig. 6 has been reported [28], where the second pole can be moved to a higher frequency without increasing g_{m2} . The improved Miller compensation is formed by adding the common-gate current buffer to the conventional Miller compensation. The phase compensation capacitor is connected between the output and the source node of the common-gate buffer. The small signal equivalent circuit of the improved Miller compensation is shown in Fig. 7. The transfer function, $H_{imc}(s)$,

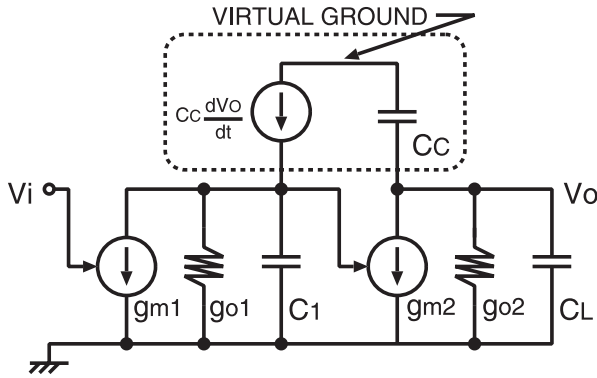


Fig. 7 Improved Miller compensation (equivalent circuit).

of the improved Miller compensation is obtained as follows;

$$H_{imc}(s) \approx A_{imc} \frac{1}{(1 - s/p_{1imc})(1 - s/p_{2imc})} \quad (7)$$

$$A_{imc} = \frac{g_{m1} g_{m2}}{g_{o1} g_{o2}} \quad (8)$$

$$p_{1imc} = -\frac{g_{o2} g_{o1}}{g_{m2} C_C} \quad (9)$$

$$p_{2imc} = -\frac{g_{m2} C_C}{C_1(C_C + C_L)} \quad (10)$$

where A_{imc} is the total DC gain, and p_{1imc} and p_{2imc} are the first and the second poles. The improved Miller compensation has two advantages over the conventional Miller compensation. One is no low-frequency zero in right-half plane, the other is a higher-frequency second pole.

In the conventional Miller compensation, there is a frequency at which the current flowing through C_C cancels the drain current of M5, i.e., a zero exists. This zero locates in the right-half-plane, and it degrades phase margin. In the improved Miller compensation, the feedforward current from the drain of M6 to the source of M6 is almost zero. This makes the zero move to very high frequency and not degrade the phase margin.

Comparing Eqs. (3) and (9), the first poles of the Miller compensation and the improved Miller compensation are almost equal. But, the second pole of the improved Miller compensation is higher than that of the conventional Miller compensation by the following ratio;

$$\frac{p_{2imc}}{p_{2mil}} = \frac{C_L C_1 + C_L C_C + C_C C_1}{C_1(C_C + C_L)} \quad (11)$$

Assuming that the opamp drives the large capacitive load, for the case of $C_1, C_C \ll C_L$, (11) can be approximated;

$$\frac{p_{2imc}}{p_{2mil}} \approx \frac{C_C}{C_1} \quad (12)$$

C_1 is usually smaller than C_C . The required C_C can be reduced to obtain the same phase margin as the conventional Miller compensation. With smaller phase compensation capacitance, it is possible to reduce the current of the input stage required for the specified slew rate (6).

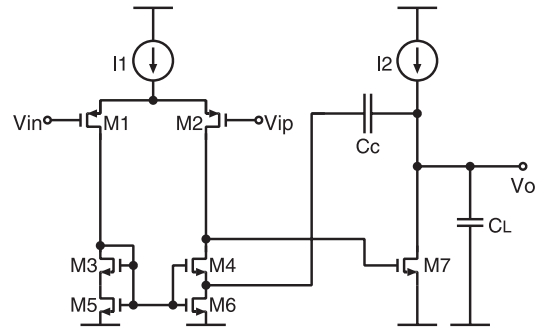


Fig. 8 Improved Miller compensation using self-cascode active load.

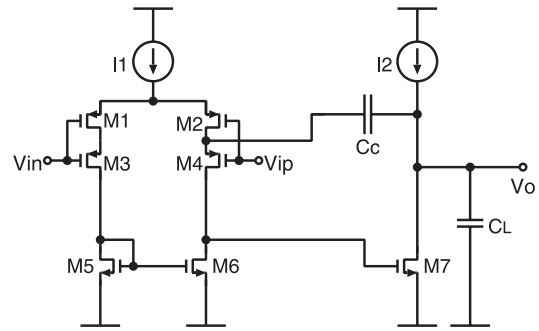


Fig. 9 Improved Miller compensation using self-cascode differential pair.

The improved Miller compensation shown in Fig. 6 requires an additional bias current. In order to apply the improved Miller compensation without increasing the current consumption, the phase compensation techniques using a self-cascode circuit have been proposed, where the self-cascode is applied to the transistor forming the active load at the input stage (Fig. 8, [5]) or the transistor forming the input differential pair (Fig. 9, [29]). In Fig. 8, the phase compensation capacitor is connected between the drain of M7 and the source of M4. M4 acts like the common-gate current buffer in Fig. 6. Since the bias current of the common-gate current buffer is shared with the bias current of the input stage, the improved Miller compensation is realized without increasing the current consumption.

The two-stage amplifier with self-cascode differential pair is shown in Fig. 9 and is suitable for the voltage follower used in the LCD driver in Fig. 3. In the voltage follower, the output node and the minus input node are connected. The input voltage is applied to the plus input node of the opamp. Because M4 in Fig. 9 operates like a source follower, the source voltage of M4 follows the input voltage. The output node changes in the same direction as the input voltage. Because the voltage across the phase compensation capacitor C_C is independent of the input voltage and is almost constant, a current from the input stage to the phase compensation capacitor C_C is little. This means that the slew rate is not limited by the phase compensation capacitor and the bias current of the input stage (6). It is possible to reduce the bias current of the input stage for achieving a required

slew rate.

In the phase compensation techniques using self-cascode circuit mentioned above, unless the multi V_{th} process is used, M5 and M6 in Fig. 8 and M1 and M2 in Fig. 9 operate in a linear region. So, all feedback current from the phase compensation capacitor C_C does not flow into the common-gate current buffer; some feedback current flows into the transistor operating in a linear region. This should be taken into account in determining the phase compensation capacitor C_C [5].

3. Phase Compensation Techniques with No On-Chip Capacitor

Even with the improved Miller compensation technique, a large Miller capacitance and/or a high g_m of the output stage is necessary to drive a large capacitive load. These two approaches still increase the power consumption of the opamp. Phase compensation techniques with no on-chip capacitor have been reported. The techniques introduce a new zero for phase compensation [30], [31].

3.1 Phase Compensation Using Capacitive Load

The introduction of zero can be realized by using the capacitive load [30]. The circuit configuration of this technique is shown in Fig. 10. A resistor is connected between the output of the opamp and the large capacitive load, and the transfer function from V_{in} to V_{out1} , $H_{ucl}(s)$, of Fig. 10 is obtained as follows;

$$H_{ucl}(s) = A_{ucl} \frac{(1 - s/z_{ucl})}{(1 - s/p_{1ucl})(1 - s/p_{2ucl})} \quad (13)$$

$$A_{ucl} = \frac{g_{m1} g_{m2}}{g_{o1} g_{o2}} \quad (14)$$

$$p_{1ucl} = -\frac{g_{o2}}{C_L} \quad (15)$$

$$p_{2ucl} = -\frac{g_{o1}}{C_1} \quad (16)$$

$$z_{ucl} = -\frac{1}{R_Z C_L} \quad (17)$$

This transfer function, $H_{ucl}(s)$, has two poles and one zero. Because this zero locates in the left-half-plane, this zero is utilized in the phase compensation. As shown in Fig. 11, the resistance R_Z is designed to insert the zero between the second pole and the unity gain frequency. Since the frequency response around the unity gain frequency becomes close to the one pole characteristic, it is possible to obtain the phase

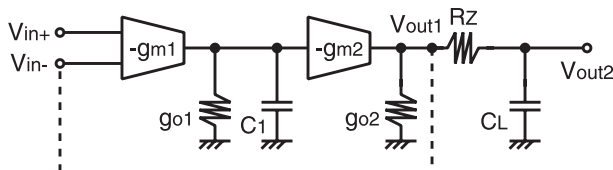


Fig. 10 Phase compensation using capacitive load.

margin. Even when the load capacitance is large, it is not necessary to increase the bias current from the viewpoint of phase compensation. This phase compensation technique with the class AB output stage is suitable for the buffer amplifier for the LCD driver to reduce the power consumption.

Note that the drive capability of the opamp is limited in R_Z and C_L . As shown in Fig. 10, the transfer function of the opamp is obtained with V_{out1} as the output node. However, the actual output node is V_{out2} where the load capacitance C_L is connected. V_{out2} becomes dull owing to LPF formed by R_Z and C_L . The high-speed phase compensation using capacitive load to alleviate the degradation due to this LPF has been proposed [31]. As shown in Fig. 12, the output stage of this circuit is formed with two parallel stages (g_{m2} and g_{m3} in Fig. 12). One output stage g_{m2} is the same configuration as Fig. 10. Another output stage g_{m3} is connected to the load capacitance C_L directly to realize a high slew rate. The transfer function, H_{hsu} , of Fig. 12 is obtained as follows;

$$H_{hsu}(s) \approx A_{hsu} \frac{(1 - s/z_{hsu})}{(1 - s/p_{1hsu})(1 - s/p_{2hsu})} \quad (18)$$

$$A_{hsu} \approx \frac{g_{m1} g_{m2} + g_{m3}}{g_{o1} g_{o2} + g_{o3}} \quad (19)$$

$$p_{1hsu} \approx -\frac{g_{o2} + g_{o3}}{C_L} \quad (20)$$

$$p_{2hsu} = -\frac{g_{o1}}{C_1} \quad (21)$$

$$z_{hsu} \approx -\frac{g_{m2} + g_{m3}}{g_{m2}} \frac{1}{R_Z C_L} \quad (22)$$

The zero indicated in (22) shifts to a higher frequency than

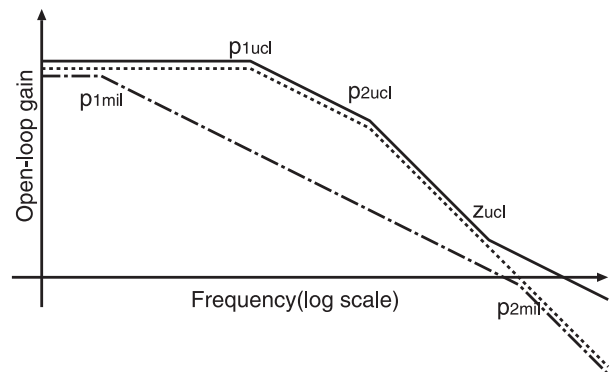


Fig. 11 Example of open-loop frequency characteristics of phase compensation using capacitive load.

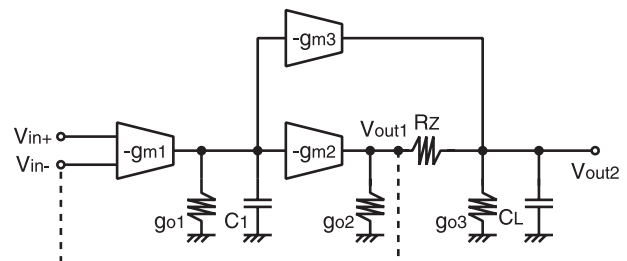


Fig. 12 High-speed phase compensation using capacitive load.

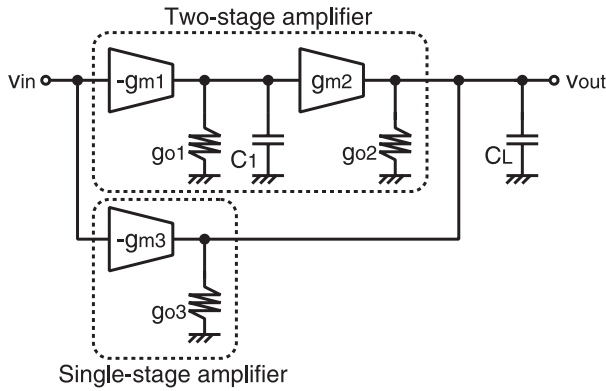


Fig. 13 No capacitor feedforward phase compensation.

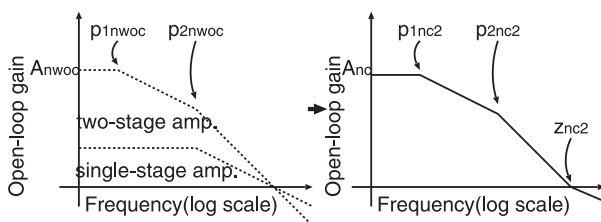


Fig. 14 No capacitor feedforward phase compensation for wideband opamp.

that indicated in (17) by the ratio of the transconductance of two output stages $(g_{m2} + g_{m3})/g_{m2}$. This shift should be taken into account in design. To insert the zero in the same frequency as the zero (17) in Fig. 10, it is necessary to increase R_Z by this ratio $(g_{m2} + g_{m3})/g_{m2}$. Because the techniques in Fig. 10 and Fig. 12 do not use the Miller capacitance, these techniques can reduce the power consumption of the input stage even when the load capacitance is large.

3.2 No Capacitor Feedforward Phase Compensation

There is the phase compensation technique suitable for wideband width that utilizes the zero without shifting the first and the second poles of the opamp to higher frequencies. This phase compensation technique needs two circuit blocks. One is the two-stage amplifiers and another is the single-stage amplifier as shown in Fig. 13. The frequency responses of these two amplifiers are combined as shown in Fig. 14. At high frequencies, the frequency response of the single-stage amplifier is dominant and vice versa at low frequencies. This means that a zero is introduced in the combined frequency response [32], [33]. The transfer function, H_{nc} , of this circuit is obtained as follows;

$$H_{nc} \approx A_{nc} \frac{(1 - s/z_{nc})}{(1 - s/p_{1nc})(1 - s/p_{2nc})} \quad (23)$$

$$A_{nc} \approx \frac{g_{m1} g_{m2}}{g_{o1} g_{o2} + g_{o3}} \quad (24)$$

$$p_{1nc} = -\frac{g_{o1}}{C_1} \quad (25)$$

$$p_{2nc} = -\frac{g_{o2} + g_{o3}}{C_L} \quad (26)$$

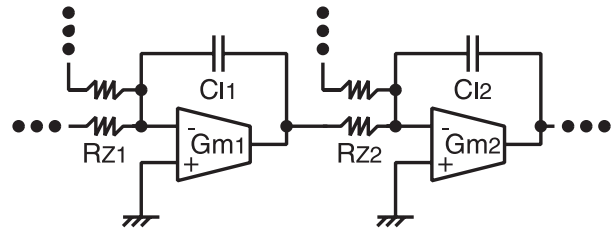


Fig. 15 The filter consists of several integrators.

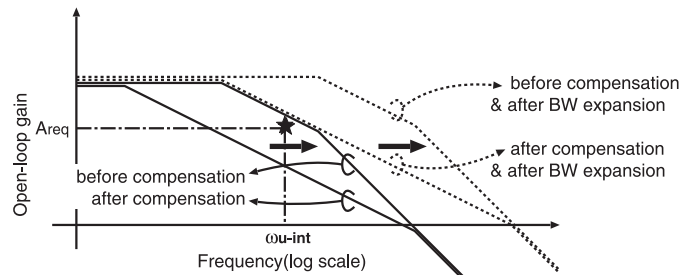


Fig. 16 Miller compensation for wideband opamp.

$$z_{nc} \approx -\frac{g_{m1}g_{m2}}{g_{m3}C_1} \quad (27)$$

This transfer function, H_{nc} , has two poles and one zero. When the unity gain frequencies of the two-stage and single-stage amplifiers are the same, the introduced zero locates at the unity gain frequency, and the phase margin is about 45° .

3.3 Comparison between Miller Compensation and No Capacitor Feedforward Phase Compensation

When the opamp is used in the LPF, the power consumption of the opamp with the Miller compensation is compared with that of the opamp with no capacitor feedforward phase compensation. The opamp is used as an integrator in the filter as shown in Fig. 15. In this configuration, the load of G_{m1} is the resistance, R_{Z2} . R_{Z2} is connected between the output of G_{m1} and the virtual short node of G_{m2} . C_{11} and R_{Z1} form the integrator with G_{m1} . A sufficient gain of the opamp around the unity gain frequency of the integrator, ω_{u-int} , is required. Here, A_{req} denotes the required gain at ω_{u-int} . Generally, the gain of the opamp at ω_{u-int} should be sufficiently large, for example, 40 dB.

In the Miller compensation, the bandwidth of the opamp after compensation should be expanded as shown in Fig. 16, when the gain at ω_{u-int} after compensation is lower than A_{req} . In the no capacitor feedforward phase compensation, although it is unnecessary to expand the bandwidth of the two-stage amplifier, the single-stage amplifier is added as shown in Fig. 13. Therefore, a current increase for expanding the bandwidth in the Miller compensation and a current increase for adding single-stage amplifier are compared. For simple calculation, the currents of the input stage and the output stage of the two-stage amplifier and the single-stage amplifier are increased to keep the current density of the transistors constant. When the current of the

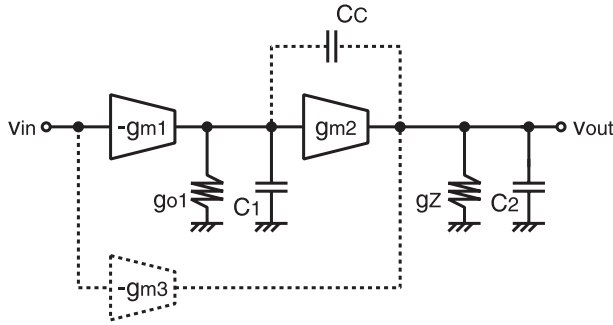


Fig. 17 Miller compensation or no capacitor feedforward phase compensation.

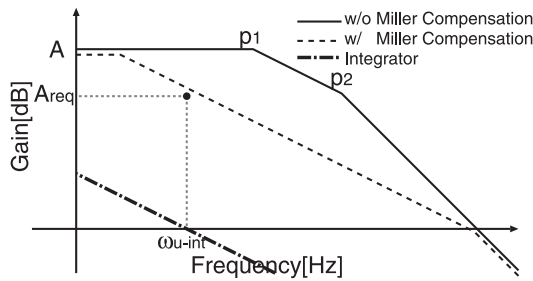


Fig. 18 Narrow bandwidth integrator with Miller compensation.

transistor increases N times, the channel width of the transistor is increased N times. Then g_m and g_o also increase N times.

Figure 17 shows a simple two-stage amplifier. g_{m1} is transconductance of the input stage, g_{m2} is transconductance of the output stage, g_{o1} is the output resistance of the input stage, g_Z denotes the load resistance as a conductance representation, C_1 is the input capacitance of the output stage, and C_2 is the output capacitance. The current consumption of the Miller compensation and no capacitor feedforward phase compensation are compared in the following two conditions; (a) ω_{u-int} is low and (b) ω_{u-int} is high.

In the first condition, ω_{u-int} is sufficiently low and the gain of the opamp at ω_{u-int} after the Miller compensation is greater than A_{req} as shown in Fig. 18. In this condition, no current increase is required when the Miller compensation is applied. On the contrary, when the no capacitor feedforward phase compensation is applied, the current increase of the additional single-stage amplifier is required. Therefore, when ω_{u-int} is sufficiently low, the Miller compensation is better than the no capacitor feedforward phase compensation.

In the second condition, ω_{u-int} is high and the gain of the opamp at ω_{u-int} after the Miller compensation is lower than A_{req} as shown in Fig. 19. In this condition, it is necessary to expand the bandwidth of the uncompensated opamp by increasing the transconductances of the input and the output stages with the current increase. The required unity gain frequency, ω_{u-req} , is obtained as follows;

$$\omega_{u-req} = A_{req}\omega_{u-int} \quad (28)$$

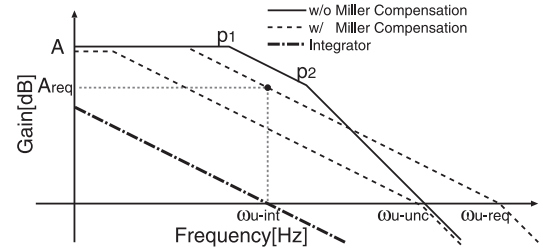


Fig. 19 Wide bandwidth integrator with Miller compensation.

The maximum unity gain frequency when the Miller compensation is applied is limited by the unity gain frequency of the uncompensated opamp, ω_{u-unc} . ω_{u-unc} is obtained as follows;

$$\omega_{u-unc} = \sqrt{\frac{g_{m1}g_{m2}}{C_1C_2}} \quad (29)$$

ω_{u-unc} should be N times expanded to satisfy Eq. (28)

$$\omega_{u-req} = N\omega_{u-unc} \quad (30)$$

$$N = A_{req}\omega_{u-int} \sqrt{\frac{C_1C_2}{g_{m1}g_{m2}}} \quad (31)$$

$$= A_{req}\omega_{u-int} \sqrt{\frac{1}{Ap_1p_2}} \quad (32)$$

where p_1 and p_2 are the first and the second poles of the uncompensated opamp. Here the current density of the transistors are assumed to be kept constant when increasing their transconductances. That is, when g_{m1} and g_{m2} are increased by L times, the currents and channel widths of the transistors in the input and the output stages are increased by L times. Then, C_1 also becomes L times larger. Therefore, when increasing ω_{u-unc} by N times, the currents of the input and the output stages should be increased by N^2 times, for example.

When the no capacitor feedforward phase compensation is applied to this opamp in this condition, the current consumption of the additional single-stage amplifier is analyzed. The unity gain frequency of the single-stage amplifier, ω_{u3} , is obtained as follows;

$$\omega_{u3} = \frac{g_{m3}}{C_2} \quad (33)$$

The ω_{u3} is designed to be the same or higher than ω_{u-unc} . The smallest g_{m3} is obtained when ω_{u3} is equal to ω_{u-unc} as shown in Fig. 20. Then the smallest g_{m3} is obtained as follows;

$$g_{m3} = \sqrt{\frac{C_2}{C_1}} g_{m1}g_{m2} \quad (34)$$

In order to express the current required for g_{m3} by using the current for g_{m2} . Equation (34) is divided by g_{m2} .

$$\frac{g_{m3}}{g_{m2}} = \sqrt{\frac{C_2}{C_1}} \frac{g_{m1}}{g_{m2}} \quad (35)$$

$$= \sqrt{\frac{A_1 p_1}{A_2 p_2}} \tag{36}$$

where A_1 and A_2 are the gains of the input and the output stages, respectively. Therefore, the required current of g_{m3} is calculated by using A_1, A_2, p_1 and p_2 .

In the Miller compensation, as ω_{u-int} is higher frequency, the required additional current becomes higher. In the no capacitor feedforward compensation, the required additional current does not depend on ω_{u-int} , and is constant as long as the gain at ω_{u-int} in uncompensated condition is greater than A_{req} . Therefore, when ω_{u-int} is sufficiently high, the no capacitor feedforward phase compensation is better than the Miller compensation.

4. Design Examples

The techniques of the phase compensation mentioned above that reduce the power consumption of the opamp are applied to the buffer amplifier for the LCD driver [34] and the opamp for the wideband LPF [35].

4.1 A Low-Power Opamp for LCD Driver

For the LCDs used in mobile terminals, low power consumption is the most important requirement. According to Ref. [30], current consumption of a few μA or less is required for the individual buffer amplifiers in the column driver. Recently, high resolution is required and the number of the signal lines on the panel has increased. Since it is physically difficult in the column driver to provide the

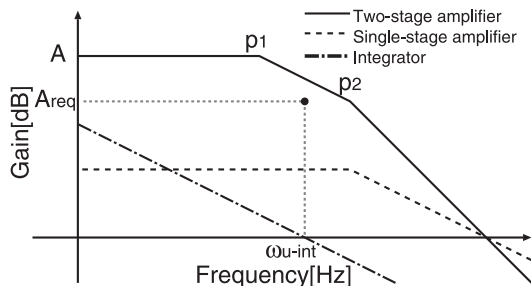


Fig. 20 Wide bandwidth integrator with no capacitor feedforward phase compensation.

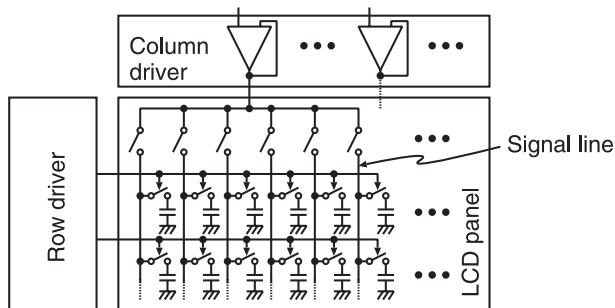


Fig. 21 Time-sharing drive.

same number of pads as the corresponding signal lines, one buffer amplifier drives plural signal lines as shown in Fig. 21, which is called time-sharing drive. In this architecture, the settling time allowed to drive one signal line becomes shorter than that in the non-time-sharing drive architecture. According to Ref. [30], the settling time is below $30 \mu sec$. When the time-sharing drive architecture is employed, the settling time becomes $4 \mu sec$ in the case that the individual buffer amplifiers drive 6 signal lines, considering the line-switching time. When 9 signal lines are driven by one buffer amplifier, the settling time becomes $2 \mu sec$.

Since a signal line on the LCD panel is capacitive, the phase compensation using capacitive load is applied. But, while switching the signal lines in the time-sharing architecture, no load is connected to the amplifier. In no load condition, it is impossible to utilize the technique of phase compensation using capacitive load. Therefore, additional phase compensation such as the Miller compensation is necessary to guarantee the stability of the amplifier in no load condition. However, when the Miller compensation capacitor is simply applied, a slew rate is limited by the Miller compensation capacitor and the bias current of the input stage. Here, the phase compensation technique suitable for the voltage follower configuration shown in Fig. 9 is applied.

In order to satisfy the requirements for the power consumption of a few μA or less, it is also important to reduce the power consumption with the improvement of drive capability of the output stage. Therefore, class AB output stage that utilizes the floating class AB control is used in the buffer amplifier [12]. The buffer amplifier for the LCD driver with the above-mentioned techniques is shown in Fig. 22 [34]. In the LCD driver, because the buffer amplifier drives the liquid crystal cell between the ground and the power supply voltage, a rail-to-rail input/output is required for the buffer amplifier. Therefore, the rail-to-rail input stage is formed by the configuration such that output currents from NMOS and PMOS differential pairs are added at the floating class AB control block.

The simulated frequency responses when the opamp drives the large capacitive load and no load are shown in Fig. 23. When the opamp drives the large capacitive load, the zero is inserted at about 1 MHz. When the opamp drives no load, the frequency response shows the normal Miller compensation response. Finally, the phase margin is 57° for

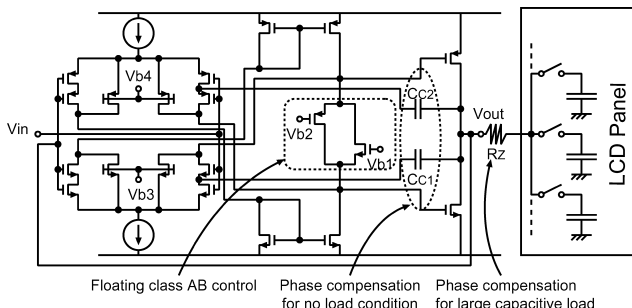


Fig. 22 Phase compensations for LCD driver.

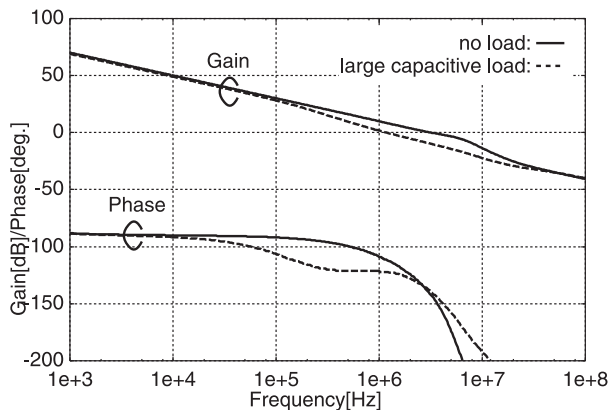


Fig. 23 Frequency responses (Simulation).

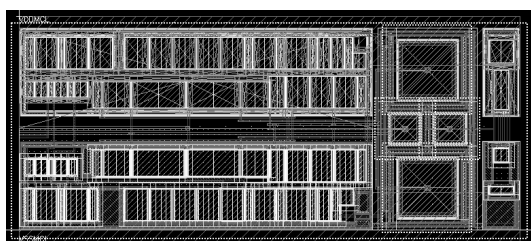


Fig. 24 Layout image of LCD driver amplifier (100 μm × 45 μm).

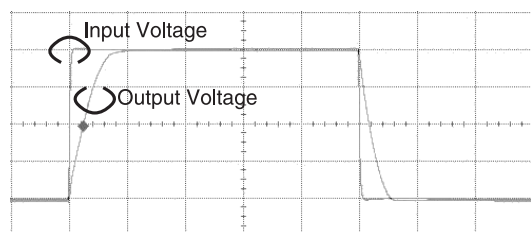


Fig. 25 Transient responses for input/output signal X-scale: 2usec/div. Y-scale: 1 V/div.(Measurement).

Table 1 Measurement summary of LCD driver amplifier.

| | |
|-------------------------------|-----------|
| Supply voltage | 5 V |
| Quiescent current consumption | 2 μA |
| Settling time at rising edge | 1.95 μsec |
| Settling time at falling edge | 1.29 μsec |
| Current consumption /line | 0.22 μA |

driving large capacitive load, and 37° for driving no load. Because two phase compensation techniques are utilized in parallel, sufficient phase margin is achieved when the opamp drives the large capacitive load and no load.

The opamp shown in Fig. 22 is fabricated with 0.13 μm CMOS process technology. A layout image is shown in Fig. 24. The layout area of the opamp is 100 μm × 45 μm without pads area. The supply voltage is 5 V, the current consumption is 2 μA. A load resistance is 10 kΩ, and a load capacitance including probe capacitance is 24 pF. When an input signal changes from 0.5 V to 4.5 V and from 4.5 V to 0.5 V, the input/output voltages are shown as in Fig. 25. The

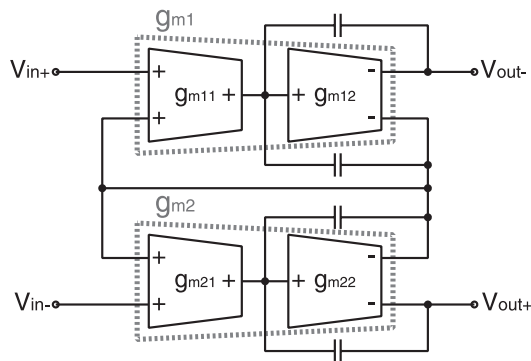


Fig. 26 Conventional balanced opamp [4].

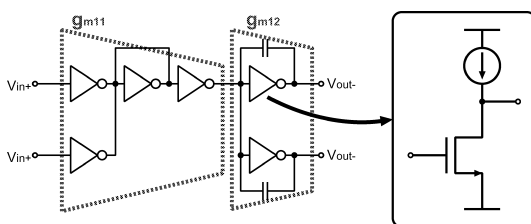


Fig. 27 Circuit configuration of gm.

settling time within ± 10 mV is 1.95 μsec at rising edge and 1.29 μsec at falling edge. The measurement summary of the opamp for LCD driver is shown in Table 1. Because both settling times are below 2 μsec, the opamp can be employed in the 9 signal lines selecting time-sharing drive architecture. Since one opamp can drive nine signal lines, the corresponding current consumption per signal line is 0.22 μA.

4.2 An Opamp for Low Supply-Voltage Wideband Filter

In the wideband wireless applications such as LTE [26] and WiMAX [27], the bandwidth of analog baseband circuit is 10 MHz. In the WLAN 802.11n [36], the bandwidth of analog baseband circuit is 20 MHz. The gate length of transistor has been decreased by improving the CMOS process technology. In finer process technologies, the maximum power supply voltage becomes lower. This deteriorates the distortion of the signal. The balanced OTA shown in Fig. 26 is suitable for low power-supply voltage, where the transconductor of the balanced OTA shown in Fig. 27 can be composed only of common-source amplifiers. In the balanced OTA, the transistor for the tail current source of differential pair shown in Fig. 4 is removed so that the minimum input voltage of the balanced OTA can be lower than the minimum input voltage of the conventional differential pair.

The Miller compensation capacitor has been applied to the conventional balanced OTA shown in Fig. 27 for the phase compensation of two-stage amplifier [4]. No capacitor feedforward compensation is applied to the balanced OTA as shown in Fig. 28 to expand the bandwidth of the balanced OTA [35]. No capacitor feedforward compensation balanced OTA is realized by the parallel connection

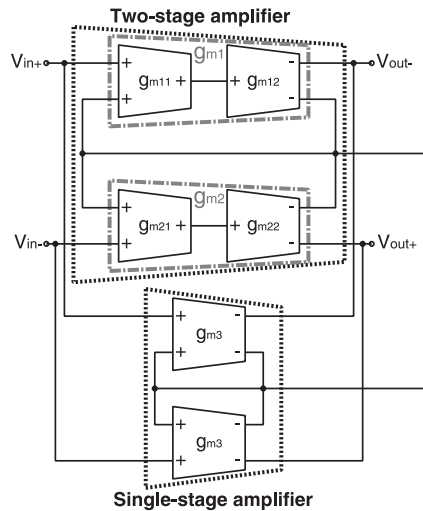


Fig. 28 No capacitor feedforward phase compensation balanced opamp.

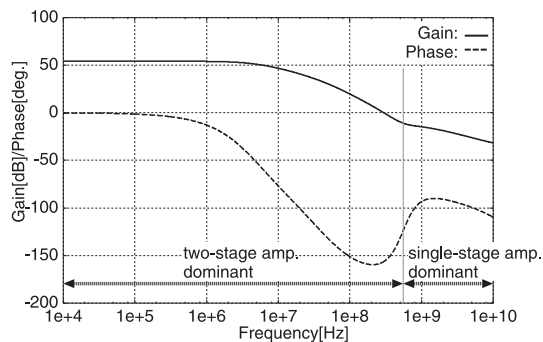


Fig. 29 No capacitor feedforward phase compensation balanced opamp's frequency characteristics (Simulation).

of two-stage balanced OTA and single-stage balanced OTA. Because the GBW for common-mode signal of the balanced OTA is the same as the GBW for differential-mode signal of the balanced OTA, it is necessary to apply the phase compensation for the common-mode signal. Because the single-stage amplifier is also composed of the balanced OTA, no capacitor feedforward compensation can be applied to the common-mode signal by connecting the common-mode feedback of the two-stage amplifier and the common-mode feedback of the single-stage amplifier. The frequency response is shown in Fig. 29. The zero is introduced at about 600 MHz. For lower frequencies than 600 MHz, the frequency response of the two-stage amplifier is dominant. For higher frequencies than 600 MHz, the frequency response of the single-stage amplifier is dominant. The phase margin of this opamp is about 25° to minimize the current increase by the single-stage amplifier. This opamp has 47 dB gain at 10 MHz.

The 5th-order Chebyshev LPF for WLAN 802.11a/b/g shown in Fig. 30 by using no capacitor feedforward compensation balanced opamp is designed with the leap-frog configuration. The frequency response of this LPF is shown in Fig. 31. The frequency response of the measurement is al-

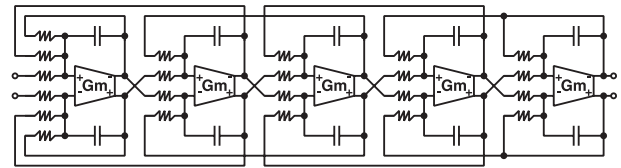


Fig. 30 5th order leap-frog low-pass filter.

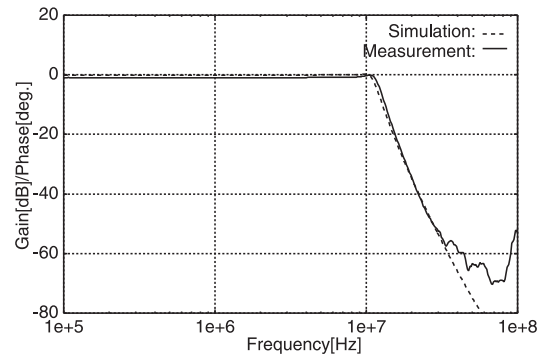


Fig. 31 Frequency response (Simulation and Measurement).

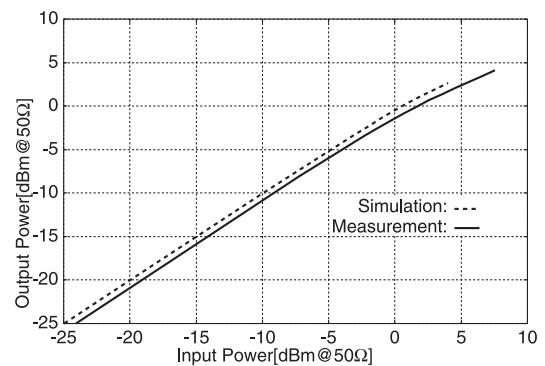


Fig. 32 P1 dB characteristic (Simulation and Measurement).

Table 2 Measurement summary of LPF.

| | |
|--|----------|
| Supply voltage | 0.9 V |
| Current consumption(5th order filter & bias) | 14.5 mA |
| Cutoff frequency | 12.2 MHz |
| Attenuation at 1st adjacent | 12.4 dB |
| IP1 dB@5 MHz | 2.78 dBm |

most equal to that of the simulation. Figure 32 shows IP1 dB of this LPF. The output voltage swing of 700 mVpp is obtained.

The analog baseband receiver circuit that operates at 0.9 V power supply can be composed by combining with Delta Sigma modulator of [4]. Table 2 shows the measurement summary.

5. Conclusions

In this paper, the phase compensation is discussed from the viewpoint of the power consumption. Depending on the applications, it should be carefully considered which

phase compensation technique is chosen. With the improved Miller compensation techniques, the compensation capacitance can be reduced, then the slew rate can be also improved without increasing the bias current. Especially for voltage follower configuration, it is realized that the compensation capacitor does not limit the slew rate in principle. The bias current can be further reduced with this compensation. In fast-settling discrete-time applications and high frequency filters, the introduction of zero is suitable for low power opamps. In the LCD column driver, the phase compensation by using the zero formed with a load capacitance is effective for power reduction. In high cut-off frequency active-RC filters, the opamp with no capacitor feedforward phase compensation dissipates lower power than the opamp with the Miller compensation. These techniques are suitable for low power and/or wideband opamps.

References

- [1] K. Lim, S.-H. Lee, S. Min, S. Ock, M.-W. Hwang, C.-H. Lee, K.-L. Kim, and S. Han, "A fully integrated direct conversion receiver for CDMA and GPS applications," *A-SSCC Dig. Tech. Papers*, pp.249–252, Nov. 2005.
- [2] J. Jussila, A. Parssinen, and K. Halonen, "A channel selection filter for a WCDMA direct conversion receiver," *Proc. ESSCIRC 2000 Conf.*, pp.236–239, Stockholm, Sept. 2000.
- [3] V. Gopinathan, M. Tarsia, and D. Choi, "Design considerations and implementation of a programmable high-frequency continuous-time filter and variable-gain amplifier in submicrometer CMOS," *IEEE J. Solid-State Circuits*, vol.34, no.12, pp.1698–1707, Dec. 1999.
- [4] T. Ueno and T. Itakura, "A 0.9 V 1.5 mW continuous-time $\Delta\Sigma$ modulator for WCDMA," *ISSCC Dig. Tech. Papers*, pp.78–79, Feb. 2004.
- [5] T. Itakura and H. Minamizaki, "10 μ A quiescent current opamp design for LCD driver ICs," *IEICE Trans. Fundamentals*, vol.E81-A, no.2, pp.230–236, Feb. 1998.
- [6] T. Itakura, "A high slew rate operational amplifier for an LCD driver IC," *IEICE Trans. Fundamentals*, vol.E78-A, no.2, pp.191–195, Feb. 1995.
- [7] P.-C. Yu and J.-C. Wu, "A class-b output buffer for flat-panel-display column driver," *IEEE J. Solid-State Circuits*, vol.34, no.1, pp.116–119, Jan. 1999.
- [8] M.-C. Weng and J.-C. Wu, "A compact low-power rail-to-rail class-b buffer for LCD column driver," *IEICE Trans. Electron.*, vol.E85-C, no.8, pp.1659–1663, Aug. 2002.
- [9] D.M. Monticelli, "A quad CMOS single-supply op amp with rail-to-rail output swing," *IEEE J. Solid-State Circuits*, vol.SC-21, no.6, pp.1026–1034, Dec. 1986.
- [10] L.G.A. Callewaert and W.M.C. Sansen, "Class AB CMOS amplifiers with high efficiency," *IEEE J. Solid-State Circuits*, vol.25, no.3, pp.684–691, June 1990.
- [11] J. Kih, B. Chang, D.-K. Jeong, and W. Kim, "Class-AB large-swing CMOS buffer amplifier with controlled bias current," *IEEE J. Solid-State Circuits*, vol.28, no.12, pp.1350–1353, Dec. 1993.
- [12] R. Hogervorst, J.P. Tero, R.G.H. Eschauzier, and H. Huijsing, "A compact power-efficient 3 V CMOS rail-to-rail input/output operational amplifier for VLSI cell libraries," *IEEE J. Solid-State Circuits*, vol.29, no.12, pp.1505–1513, Dec. 1994.
- [13] F. You, S.H.K. Embabi, and E. Sanchez-Sinencio, "Low-voltage class AB buffers with quiescent current control," *IEEE J. Solid-State Circuits*, vol.33, no.6, pp.915–920, June 1998.
- [14] V. Peluso, P. Vancorenland, A.M. Marques, M.S.J. Steyaert, and W. Sansen, "A 900-mV low-power $\Delta\Sigma$ A/D converter with 77-dB dynamic range," *IEEE J. Solid-State Circuits*, vol.33, no.12, pp.1887–1897, Dec. 1998.
- [15] T.Y. Man, P.K.T. Mok, and M. Chan, "A high slew-rate push-pull output amplifier for low-quiescent current low-dropout regulators with transient-response improvement," *IEEE Trans. Circuits Syst. II, Express Briefs*, vol.54, no.9, pp.755–759, Sept. 2007.
- [16] C.-H. Lin, K.-H. Chen, and H.-W. Huang, "Low-dropout regulators with adaptive reference control and dynamic push-pull techniques for enhancing transient performance," *IEEE Trans. Power Electron.*, vol.24, no.4, pp.1016–1022, April 2009.
- [17] L. Koushaeian, R. Amirkhanzadeh, and A. Zayegh, "Dynamic biasing current source for highly linear OTA with constant transconductance and wide input common-mode range," *Proc. TENCON*, pp.1–4, Nov. 2008.
- [18] H.-L. Chen, Y.-S. Lee, and J.-S. Chiang, "Low power sigma delta modulator with dynamic biasing for audio applications," *Proc. MWSCAS*, pp.159–162, Aug. 2007.
- [19] B.J. Hosticka, "Dynamic CMOS amplifiers," *IEEE J. Solid-State Circuits*, vol.SC-15, no.5, pp.881–886, Oct. 1980.
- [20] V.R. Saari, "Low-power high-drive CMOS operational amplifier," *IEEE J. Solid-State Circuits*, vol.SC-18, no.1, pp.121–127, Feb. 1983.
- [21] R. Klinke, B.J. Hosticka, and H.-J. Pfeleiderer, "A very-high-slew-rate CMOS operational amplifier," *IEEE J. Solid-State Circuits*, vol.24, no.3, pp.744–746, June 1989.
- [22] K. Nagaraj, "CMOS amplifiers incorporating a novel slew rate enhancement technique," *Proc. IEEE CICC*, pp.11.6/1–11.6/5, 1990.
- [23] R.G.H. Eschauzier, L.P.T. Kerklaan, and J.H. Huijsing, "A 100-MHz 100-dB operational amplifier with multipath nested Miller compensation structure," *IEEE J. Solid-State Circuits*, vol.27, no.12, pp.1709–1717, Dec. 1992.
- [24] R.G.H. Eschauzier, R. Hogervorst, and J.H. Huijsing, "A programmable 1.5 V CMOS Class-AB operational amplifier with hybrid nested Miller compensation for 120 dB gain and 6 MHz UGF," *IEEE Trans. Solid-State Circuits*, vol.29, no.12, pp.1497–1504, Dec. 1994.
- [25] X. Fan, C. Mishra, and E. Sanchez-Sinencio, "Single miller capacitor frequency compensation technique for low-power multistage amplifiers," *IEEE J. Solid-State Circuits*, vol.40, no.3, pp.584–592, March 2005.
- [26] J. Berkman, C. Carbonelli, F. Dietrich, C. Drewes, and W. Xu, "On 3G LTE terminal implementation — Standard, algorithms, complexities and challenges," *Proc. IWCMC*, pp.970–975, 2008.
- [27] M. Locker, M. Tomesen, J. Kuonen, A. Daanen, H. Visser, B. Essink, P.P. Vervoort, M. Nijrolder, R. Kopmeiners, W. Redman-White, R. Balmford, and R.E. Waffaoui, "A low power, high performance BiCMOS MIMO/diversity direct conversion transceiver IC for WiBro/WiMAX (802.16e)," *Proc. IEEE CICC*, pp.101–105, 2007.
- [28] B.K. Ahuja, "An improved frequency compensation technique for CMOS operational amplifier," *IEEE J. Solid-State Circuits*, vol.SC-18, no.6, pp.629–633, Dec. 1983.
- [29] T. Itakura and T. Iida, "A simple phase compensation technique with improved PSRR for CMOS opamps," *IEICE Trans. Fundamentals*, vol.E83-A, no.6, pp.941–948, June 2000.
- [30] T. Itakura, H. Minamizaki, T. Saito, and T. Kuroda, "A 402-output TFT-LCD driver IC with power control based on the number of colors selected," *IEEE J. Solid-State Circuits*, vol.38, no.3, pp.503–510, March 2003.
- [31] C.-W. Lu, "High-speed driving scheme and compact high-speed low-power rail-to-rail class-b buffer amplifier for LCD applications," *IEEE J. Solid-State Circuits*, vol.39, no.11, pp.1938–1947, Nov. 2004.
- [32] J. Harrison and N. Weste, "A 500 MHz CMOS anti-alias filter using feed-forward op-amps with local common-mode feedback," *ISSCC Dig. Tech. Papers*, pp.132–483, Feb. 2003.
- [33] B.K. Thandri and J. Silva-Martinez, "A robust feedforward compensation scheme for multistage operational transconductance amplifiers with no Miller capacitors," *IEEE J. Solid-State Circuits*, vol.38,

no.2, Feb. 2003.

- [34] R. Ito, T. Itakura, and H. Minamizaki, "A class AB amplifier for LCD driver," IEEE Digest of Tech. Papers, Symposium on VLSI Circuits, pp.148–149, June 2007.
- [35] R. Ito and T. Itakura, "A study of baseband filter for the low supply voltage and the wideband signal," IEICE General Conference, A-1-15, p.15, March 2007.
- [36] S. Kousai, M. Hamada, R. Ito, and T. Itakura, "A 19.7 MHz, fifth-order active-RC chebyshev LPF for draft IEEE802.11n with automatic quality-factor tuning scheme," IEEE J. Solid-State Circuits, vol.42, no.11, pp.2326–2337, Nov. 2007.



Rui Ito received the B.E. and M.E. degrees from Kanagawa University, Yokohama, in 2000 and 2002, respectively. In 2002 he joined the Corporate Research & Development Center, Toshiba Corporation, Kanagawa. He is now with the Toshiba Corporation Semiconductor Company, Kawasaki. His research interests include analog IC design for telecommunication and LCD driver ICs.



Tetsuro Itakura received the B.E. degree from the Tokyo University of Agriculture and Technology, Tokyo, in 1981, the M.S. degree from Stanford University, Stanford, CA, in 1989, and the Doctor of Engineering degree from Tokyo Institute of Technology, Tokyo, in 2003. In 1981, he joined Toshiba Corporation, Kawasaki, where he is with the Wireless System Laboratory, Corporate Research and Development Center. He has been engaged in the research and development of analog integrated circuits for telecommunications and for LCD driver ICs. His current interests

are analog LSI design and signal processing.